1999

X-ray emission from the local supercluster: possible evidence for hot, diffuse gas

Stephen P. Boughn
Haverford College, sboughn@haverford.edu

THE ASTROPHYSICAL JOURNAL, 526:14–26, 1999 November 20

X-RAY EMISSION FROM THE LOCAL SUPERCLUSTER: POSSIBLE EVIDENCE FOR HOT, DIFFUSE GAS

STEPHEN P. BOUGHN
Department of Astronomy, Haverford College, Haverford, PA 19041; sboughn@haverford.edu
Received 1998 July 27; accepted 1999 July 7

ABSTRACT

The *HEAO 1* A2 full sky, 2–10 keV X-ray map was searched for emission correlated with the plane of the Local Supercluster of galaxies. After removing strong point and moderately extended sources (e.g., the core of the Virgo cluster), there remained a statistically significant component of "diffuse" X-rays in the plane of the supercluster. Fitting this diffuse component with a simple "pillbox" model of the local supercluster implies a volume X-ray emissivity of $\varepsilon_X = 3.0 \pm 0.3 \times 10^{39}(R_{SC}/20\ \mathrm{Mpc})^{-1}$ ergs s^{-1} Mpc^{-3}, where R_{SC} is the radius of the supercluster and the error is photon counting noise only. If one considers fluctuations in the X-ray background as an additional component of noise, then the detection is reduced considerably to 2.3 σ. However, the significance level implied by this value (i.e., 99%) is consistent with the distribution of fits to the model obtained by rotating the original data. If the source of the X-ray emission is bremsstrahlung from a uniformly distributed plasma with temperature T_e, then the implied electron number density is $N_e = 2.5 \times 10^{-6}(R_{SC}/20\ \mathrm{Mpc})^{-1/2}(kT_e/10\ \mathrm{keV})^{-1/4}$ cm^{-3}. This value is about an order of magnitude larger than the average baryon number density implied by nucleosynthesis and is consistent with a collapse factor of 10. A search for similar structure in the *COBE* 53 GHz microwave background map yielded a marginal detection with an amplitude of $\sim -17 \pm 5$ μK (statistical error only), which is consistent with the Sunyaev-Zeldovich (SZ) effect expected from 10 keV gas. This latter value is comparable to the amplitude of intrinsic large-scale fluctuations in the microwave background and should be considered to be a 1 σ result at best.

Subject headings: diffuse radiation — large-scale structure of universe — X-rays: galaxies — X-rays: general

1. INTRODUCTION

The largest known structures in the clustering hierarchy of galaxies are flattened distributions known as "superclusters" (SCs). The Local Supercluster (LSC), the supercluster of which the Galaxy is a member, was initially discussed by de Vaucouleurs (1953). Since then catalogs containing hundreds of SCs have been compiled (Bahcall & Soneira 1984; Batuski & Burns 1985; Einasto et al. 1997). Although it seems likely that many, if not most, SCs are gravitationally bound structures, they are far from virialized. Nevertheless, Small et al. (1998) have recently used virial-type arguments to place a lower limit on the mass of the Corona Borealis SC. The fact that SCs are only marginally overdense, i.e., $\delta\rho/\rho \sim 10$, further complicates studies of their structures. While the study of SCs is in its infancy, these objects promise to provide important information about the formation of large-scale structure in the universe.

If little is known about the dynamics of SCs, even less is known about the intrasupercluster (ISC) medium. Assuming SCs have baryon-to-light ratios comparable to rich clusters of galaxies, one expects a substantial amount of ISC gas. Furthermore, the virial temperatures of SCs are $\sim 10^8$ K, so it would not be surprising to find "hard" (>1 keV) X-ray emission from the ISC medium as is the case for the intergalactic medium in rich clusters of galaxies. Most models of structure formation predict the presence of a hot ISC, whether it is primordial, created from winds from an early population of stars, or tidally stripped from merging structures (Molnar & Birkinshaw 1998, and references cited therein). Estimated temperatures range from 10^6 to 10^8 K (Klypin & Kates 1991; Rephaeli & Persic 1992; Metzler & Evrard 1994; Anninos & Norman 1996; Cen & Ostriker 1999). It is straightforward to show that the cooling time for such gas at the expected densities ($<10^{-3}$ cm^{-3}) is much longer than a Hubble time (Rephaeli & Persic 1992), so it would remain hot today.

There have been several searches for diffuse X-ray emission from SCs. Although Murray et al. (1978) claimed that *Uhuru* data showed evidence for ISC emission, subsequent observations and analyses have not supported this claim (Pravdo et al. 1979; Persic, Rephaeli, & Boldt 1988; Persic et al. 1990). Using *ROSAT* PSPC data, Bardelli et al. (1996) reported the detection of diffuse emission in the region between two clusters in the Shapley supercluster. On the other hand, Day et al. (1991) and Molnar & Birkinshaw (1998) have placed relatively strong upper limits on the 2–10 keV diffuse emission in this supercluster. While the current upper limits are interesting, they still leave room for a substantial amount of hot ISC matter, and more sensitive searches are underway. Particularly intriguing is the result from the cross-correlation analysis of the *ROSAT* All-Sky Survey with the Abell catalog. Soltan et al. (1996) found that Abell clusters seemed to be associated with diffuse X-ray emission with an extent of $\sim$20 Mpc. It is tempting to associate this emission with hot ISC gas, although there is as yet no direct evidence for this.

Hot ISC gas can also leave its signature on the cosmic microwave background (CMB) via the Sunyaev-Zeldovich (SZ) effect. Hogan (1992) suggested that the SZ effect in superclusters might account for the fluctuations in the CMB observed by the *COBE* satellite; however, subsequent analyses have shown that this is not the case (Boughn & Jahoda 1993; Bennett et al. 1993). Molnar & Birkinshaw (1998) used the lack of an SZ effect in the *COBE* Differential

Microwave Radiometer (DMR) data to place an additional constraint on the ISC gas in the Shapley supercluster, and Banday et al. (1996) found no evidence for the SZ effect in superclusters using a statistical cross-correlation analysis. Because of the large intrinsic fluctuations in the CMB, searches for the SZ effect in SCs will undoubtedly result in upper limits until the next generation of CMB satellites provide adequate frequency coverage to resolve the two effects.

Searches for ISC gas in the local supercluster (LSC) having the advantage of much higher integrated signal, however, are frustrated by the presence of other large-scale structure in the X-ray sky. Shafer (1983) and Boldt (1987) reported evidence for large-scale structure in the *HEAO 1* A2 2–10 keV data that is roughly consistent with either the Compton-Getting dipole expected from the Earth's motion with respect to the CMB or general emission from the direction of the center of the LSC. Subsequent analyses (Shafer & Fabian 1983) demonstrated that Compton-Getting dipole adequately accounts for this large-scale structure; however, the direction of the dipole was determined to be in a somewhat different direction than that of the CMB dipole. Jahoda & Mushotzky (1989) found evidence for enhanced 2–10 keV emission from the direction of the Great Attractor, which is in the same general direction as the Compton-Getting dipole. In addition, Jahoda (1993) has found evidence for high-latitude 2–10 keV emission from the Galaxy as well as emission associated with the superglactic plane (the plane of the LSC), the latter of which is particularly relevant to the analysis presented in this paper.

In the following sections we present evidence that there is enhanced emission in the supergalactic plane and that this emission is distinct from the other large-scale structures indicated above. To be sure, the effect is evident only at the 2.3 σ level; however, we demonstrate by independent means that it is significant at the 99% confidence level. If the X-ray emission is present at the suggested level, we will argue that the bulk of this emission is diffuse and not associated with galaxies or other compact X-ray sources in the plane. It is, of course, possible that the emission is due to still larger scale structure of the type discussed by Miyaji & Boldt (1990) and Lahav, Piran, & Treyer (1997) or even to the chance alignment of fluctuations in the X-ray background (XRB), although we argue that the latter is unlikely. These possibilities will be discussed in more detail below.

2. *HEAO 1* A2 2–10 keV X-RAY MAP

The *HEAO 1* A2 experiment measured the surface brightness of the X-ray background in the 0.1–60 keV band (Boldt 1987). The present data set was constructed from the output of two medium-energy detectors (MEDs) with different fields of view ($3° \times 3°$ and $3° \times 1.°5$) and two high-energy detectors (HED3) with these same fields of view. The data were collected during the six month period beginning on day 322 of 1977. Counts from the four detectors were combined and binned in 24,576 $1.°3 \times 1.°3$ pixels in an equatorial quadrilateralized spherical cube projection on the sky (White & Stemwedel 1992). The combined map has a spectral bandpass (quantum efficiency $\gtrsim 50\%$) of approximately 3–17 keV (Jahoda & Mushotzky 1989) and is shown in Galactic coordinates in Figure 1. For consistency with previous work, all signals will be converted to equivalent flux in the 2–10 keV band.

The effective point spread function (PSF) of the map was determined by averaging the PSFs of 75 *HEAO 1* point sources (Piccinotti et al. 1982). The composite PSF is well fitted by a Gaussian with a full width at half-maximum of $2.°96$. This value will be important in estimating the effective noise in the maximum likelihood fits of § 3.4. Because of the pixelization, the PSF varies somewhat with location on the sky; however, this has little effect on noise estimates, so we assume a constant PSF.

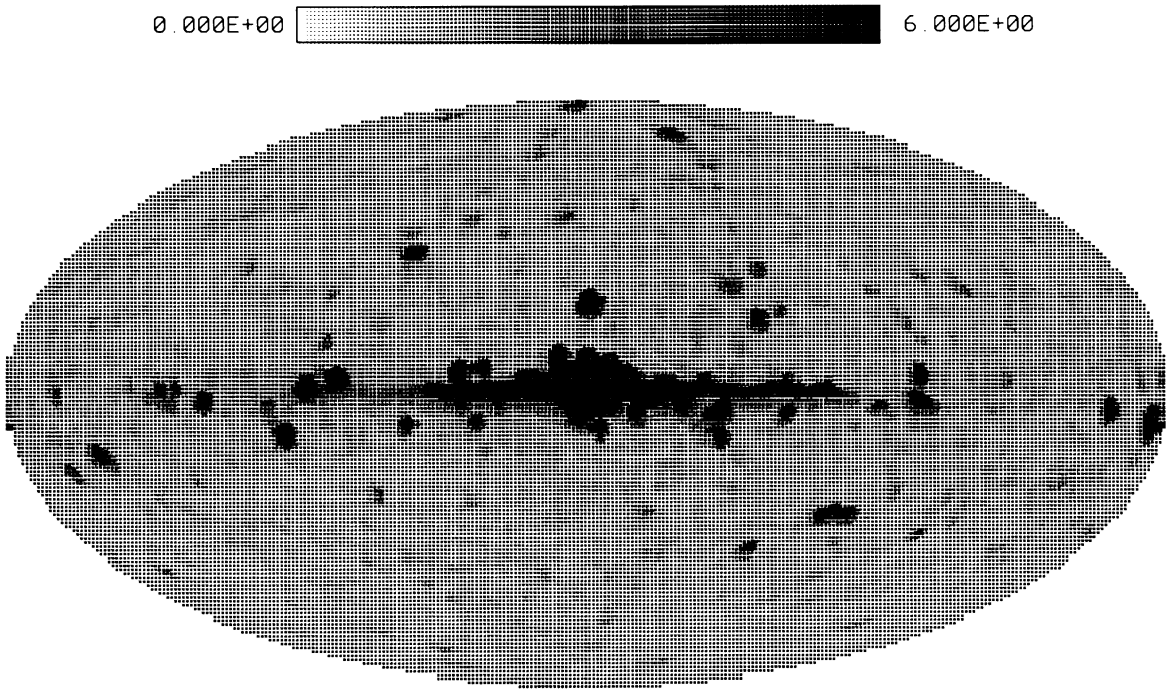

FIG. 1.—2–10 keV *HEAO 1* A2 map in Galactic coordinates (Jahoda & Mushotzky 1989). The units are TOT counts s^{-1} (see text).

In order to remove the effects of both points source and large-scale structure, more than half the map was flagged and not included in the fits described in § 3. The dominant feature in the *HEAO* map is the Galaxy (see Fig. 1), so all data within 20° of the Galactic plane and, in addition, within 30° of the Galactic center were cut from the map. In addition, 10° diameter regions around 90 discrete X-ray sources with 2–10 keV fluxes larger than 3×10^{-11} ergs s^{-1} cm^{-2} (Piccinotti et al. 1982) were removed. The resulting "cleaned" map covered about 50% the sky. In order to identify additional point sources, the map itself was searched for "sources" that exceeded the nearby background by a specified amount. This was accomplished by first averaging each pixel with its eight neighbors (note that the quadrilaterized cube format lays out the pixels on an approximately square array) and then comparing this value with the median value of the next nearest 16 pixels. Pixels within the flagged Galactic region are ignored. If the average flux associated with a given pixel exceeds the median flux of the background by a prescribed amount, then all 25 pixels are flagged and removed from further consideration. These flagged regions correspond approximately to a $6.^{\circ}5 \times 6.^{\circ}5$ patch. This procedure is not done iteratively; i.e., each comparison is made on the basis of the original map with only the Galaxy flagged. Cuts were made at several levels corresponding to average fluxes of from 3 to 7×10^{-12} ergs s^{-1} cm^{-2}. The most extreme cut corresponds to an equivalent point source flux of 3×10^{-11} ergs s^{-1} cm^{-2} and results in 75% of the sky being flagged. At this level, most of the "sources" cut are either noise fluctuations or fluctuations in the X-ray background. In any case, the results of § 3.5 are largely insensitive to these cuts.

Only one large-scale correction to the map, the Compton-Getting dipole, was made a priori. If the dipole moment of the cosmic microwave background is a kinematic effect, as it has been widely interpreted (Bennett et al. 1996), then the X-ray background should possess a similar dipole structure (Compton-Getting effect) with an amplitude of 4.3×10^{-3}. As discussed in § 1, evidence for this structure is found in the *HEAO* map (Shafer 1983; Shafer & Fabian 1983; Lahav et al. 1997). The cleaned map was corrected for this effect; however, the results of § 3.5 are the same even if the amplitude and direction of the dipole are fitted from the data.

The presence of three other sources of large-scale structure in the X-ray map has been noted. A linear time drift in detector sensitivity (Jahoda 1993) results in effective large-scale structure of known form but unknown amplitude. In addition, the 2–10 keV background shows evidence of high-latitude Galactic emission as well as emission associated with the supergalactic plane (Jahoda 1993). Models for all three of these contributions are simultaneously fitted to the data as is discussed in § 3.4.

Because of the ecliptic longitude scan pattern of the *HEAO* satellite, sky coverage and, therefore, photon shot noise are not uniform. However, the mean variance of the cleaned, corrected map, 2.0×10^{-2}(TOT counts s^{-1})^2, is considerably larger than the mean variance of photon shot noise, 0.67×10^{-2}(TOT counts s^{-1})^2, where 1 TOT counts $s^{-1} \approx 2.1 \times 10^{-11}$ ergs s^{-1} cm^{-2} (Allen, Jahoda, & Whitlock 1994). This implies that the X-ray map is dominated by "real" structure (not photon shot noise). For this reason, we chose to weight the pixels equally in all subsequent analyses.

3. MODELING THE LARGE-SCALE STRUCTURE

3.1. *Instrument Drift*

At least one of the A2 detectors changed sensitivity by $\sim 1\%$ in the six month interval of the current data set (Jahoda 1993). Because of the ecliptic scan pattern of the *HEAO* satellite, this results in a large-scale pattern in the sky that varies with ecliptic longitude with a period of 180°. If the drift is assumed to be linear, the form of the resulting large-scale structure in the map is completely determined. A linear drift of unknown amplitude is taken into account by constructing a sky map with the appropriate structure and then fitting for the amplitude simultaneously with the other parameters. We investigated the possibility of nonlinear drift by considering quadratic and cubic terms as well; however, the results of § 3.5 are insensitive to this refinement.

3.2. *The Galaxy*

The X-ray background has a diffuse (or unresolved) Galactic component that varies strongly with Galactic latitude (Iwan et al. 1982). This emission is still significant at high Galactic latitude ($b > 20°$) and extrapolates to $\sim 1\%$ at the Galactic poles. We modeled this emission in two ways. The first model consisted of a linear combination of a secant-law Galaxy with the Haslam 408 GHz full sky map (Haslam et al. 1982). The latter was included to take into account X-rays generated by inverse Compton scattering of CMB photons from high-energy electrons in the Galactic halo, the source of much of the synchrotron emission in the Haslam map. We find only marginal evidence for such emission (§ 3.5). As an alternative Galaxy model, we also considered the two-disk, exponentially truncated model of Iwan et al. (1982). The analysis of § 3.5 shows significant X-ray emission correlated with either of these models.

3.3. *The Local Supercluster*

The level of emission from the plane of the LSC reported in this paper is barely above the noise (S/N = 2.3). Therefore, detailed models of LSC emission are not particularly useful. We chose a simple "pillbox" model, i.e., uniform X-ray emissivity, ε_X, within a circular disk of radius R_{SC} and height (thickness) H_{SC}. The X-ray intensity in a particular direction is then proportional to the path length, L, through the LSC disk, i.e., $I_X = \varepsilon_X L/4\pi$. The nominal location of the LSC disk was chosen to be in the supergalactic plane (Tully 1982) with a nominal center in the direction of the Virgo cluster (M87); however, these positions were allowed to vary from their fiducial locations. The radial position of the Galaxy was assumed to be $0.8R_{SC}$ from the center of the LSC, i.e., near the edge. The value of R_{SC} is left as a scale parameter in the final results; however, the dependence on the diameter of the LSC was investigated by varying the radial position of the Galaxy within the LSC disk (see § 4.5). The thickness to diameter ratio, $H_{SC}/2R_{SC}$, was also varied; however, we considered the nominal value to be 1/8, which is consistent with the distribution of galaxies in the LSC (Tully 1982). In any case, as is true for the Galaxy model, the results of § 3.5 are not overly sensitive to these model parameters.

3.4. *Analysis*

Combining the three above models with a uniform X-ray background we arrive at the following five-parameter

expression for the "diffuse" X-ray intensity, X_i, in the $i^{\rm th}$ sky pixel,

$$X_i = a_1 + a_2 \times P_i + a_3 \times T_i + a_4 \times S_i + a_5 \times H_i\,, \quad (1)$$

where the first term represents the intensity of the uniform X-ray background, P_i represents the intensity due to the LSC pillbox normalized to a path length of $1R_{\rm SC}$, T_i is the pattern on the sky caused by a linear drift in detector sensitivity, S_i is emission proportional to the cosecant of Galactic latitude normalized to the Galactic pole, H_i is the antenna temperature (in kelvins) of the 408 MHz Haslam map, and a_k are the five free parameters. P_i, S_i, and H_i are convolved with the PSF of the observed map. Since, as discussed above, each pixel was weighted equally, the least-squares fit to the five parameters is obtained by minimizing an effective χ^2,

$$\chi^2 = \sum_i \left(x_i - \sum_m a_m X_{m,i} \right)^2 , \quad (2)$$

where x_i is the observed X-ray intensity in the $i^{\rm th}$ pixel, $X_{m,i}$ is the $i^{\rm th}$ pixel of the $m^{\rm th}$ parameter map (i.e., $X_{1,i} = 1$, $X_{2,i} = P_i$, $X_{3,i} = T_i$, $X_{4,i} = S_i$, and $X_{5,i} = H_i$), and a_m is the $m^{\rm th}$ fit parameter. The sum, $\sum_i$, is over all unflagged pixels in the cleaned *HEAO* map.

The errors in the fit due to uncorrelated shot noise are easily computed by (see for example Press et al. 1986, p. 509)

$$\sigma_k^2 = \sum_{m,\,n} \boldsymbol{C}_{k,m}\, \boldsymbol{C}_{k,n} \sum_i \sigma_i^2\, X_{m,i}\, X_{n,i}\,, \quad (3)$$

where $1 \le k, m, n \le 5$ indicate the five fit parameters and σ_i indicates the photon shot noise in the $i^{\rm th}$ pixel. $\boldsymbol{C}_{m,n}$ is the inverse of the matrix $\boldsymbol{A}_{m,n}$, which is defined as $\boldsymbol{A}_{m,n} = \sum_i X_{m,i} X_{n,i}$.

The intrinsic fluctuations in the X-ray background (XRB) can be thought of as an additional source of noise. The errors in the fit parameters induced by this noise are more problematic since XRB fluctuations exhibit pixel to pixel correlations due to the finite PSF of the detectors and the clustering of X-ray sources. In addition, these fluctuations may not be uniform on the sky. If $R_{i,i'} = \langle \delta I_{{\rm X},i}\, \delta I_{{\rm X},i'} \rangle$ represents the autocorrelation function (ACF) of the intensity of the XRB, then it is straightforward to show that the corresponding errors in the fit parameters are given by

$$\sigma_k'^2 = \sum_{m,n} \boldsymbol{C}_{k,m}\, \boldsymbol{C}_{k,n} \sum_{i,i'} R_{i,i'}\, X_{m,i}\, X_{n,i'}\,. \quad (4)$$

As an estimate of these errors we will, in the analysis to follow, assume that the fluctuations are uniform. This assumption was checked after the fact by evaluating the postfit residual rms fluctuations. After accounting for photon counting noise, there is no evidence for significant variation of the intrinsic fluctuations across the sky. In particular, the rms sky fluctuations near the plane of the LSC was within 3% of the rms over the entire sky. Figure 2 is the ACF of the X-ray map (map 2; see § 3.5) corrected for large-scale structure (i.e., a uniform X-ray background, the Compton-Getting dipole, Galaxy and LSC emission, and instrumental drift). The point at $\theta = 0$ has been corrected for photon shot noise. If correlated structure on small angular scales is entirely due to a Gaussian PSF, i.e., PSF $\propto \sim \exp(-\theta^2/2\sigma_f^2)$ it is straightforward to show that the ACF has the form $R_{i,i'} = R_0 \sim \exp(\theta_{i,i'}^2/4\sigma_p^2)$, where $\theta_{i,i'}$ is the angle between the $i^{\rm th}$ and the $i'^{\rm th}$ pixels. The dashed curve in Figure 2 is this functional form. Note that σ_p is not a fit parameter but is determined by the profiles of point sources (see § 2). While this curve is a good fit to the data for $\theta < 4°$, the data for $4° \lesssim \theta \lesssim 10°$ lie somewhat above the curve. Whether or not this is due to clustering of the X-ray background or to an improperly modeled PSF is not clear; however, it seems unlikely that the PSF extends out to 10°. In any case, we have also modeled the ACF as the sum of an exponential and a term proportional to $(\theta^2 + \theta_o^2)^{-1}$ to account for the possibility of large-scale clustering. The solid curve in Figure 2 represents this four-parameter fit.

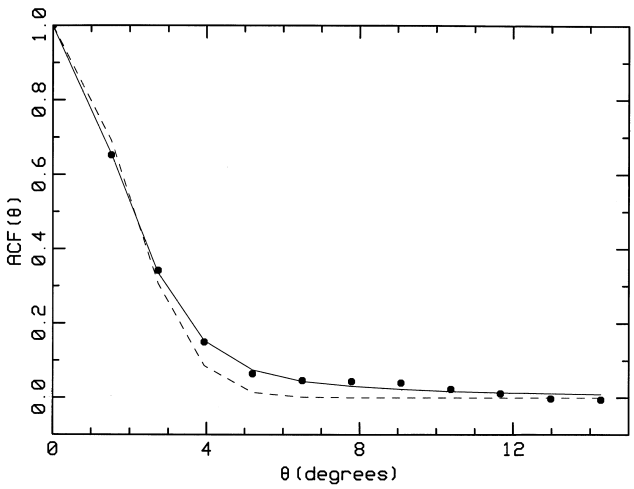

FIG. 2.—Autocorrelation function (normalized to unity) of map 2 (see § 3.5) corrected for large-scale structure. The dashed curve is that expected for the Gaussian PSF of the map. The solid curve is a fit to the data to account for the tail of the ACF (see text).

Since the photon shot noise and sky fluctuations are uncorrelated, the two sources of errors should be added in quadrature, i.e., $\sigma_{\rm tot}^2 = \sigma^2 + \sigma'^2$.

3.5. *Results*

The results of the analysis described in § 3.4 for two different cleaning windows of the map are given in Table 1. Map 1 is minimally windowed; i.e., the Galaxy pixels are flagged as well as the regions around the Piccinotti sources (see § 2). In addition, 20 "sources," i.e., isolated regions of high flux, were flagged (see § 2); however, these comprised only 0.21 sr, i.e., 1.6% of full sky. This cleaned map contains 11,637 pixels, which corresponds to a 47% sky coverage. Map 2 was subjected to more aggressive source cleaning and contains 8153 pixels, i.e., 33% sky coverage.

The three errors listed in Table 1 are for photon shot noise only and for shot noise plus the estimated noise for fluctuations in the XRB according to the two models of Figure 2 (see § 3.4). For shot noise alone, χ_ν^2 is quite large, which is simply an indication of the importance of fluctuations in the XRB. When these fluctuations are included χ_ν^2 drops considerably. The fact that in the latter case $\chi_\nu^2 \sim 1$ is not particularly significant since fluctuations in the XRB were estimated from excess noise in the map. The effective number of degrees of freedom is considerably less (by a factor of 6.8 for map 2) than the number of pixels since the largest component of the noise is correlated.

It is clear from Table 1 that the parameters from the two fits are consistent with each other and that all parameters except a_5 are significantly different from zero. From Table 2 we see that fit parameters are not strongly correlated with each other. Of particular significance to this paper is that

TABLE 1

FIT PARAMETERS FOR MAPS 1 AND 2

	Map 1				Map 2			
k	a_k	σ_a	σ_b	σ_c	a_k	σ_a	σ_b	σ_c
1.....	328.17	0.36	1.30	1.49	329.06	0.42	1.49	1.73
2.....	3.38	0.29	1.06	1.18	3.16	0.34	1.21	1.37
3.....	6.38	0.29	0.99	1.06	6.26	0.34	1.15	1.30
4.....	3.23	0.18	0.64	0.70	2.25	0.21	0.74	0.84
5.....	0.10	0.01	0.05	0.05	0.06	0.02	0.05	0.06
χ_ν^2		3.57	0.99	0.99		2.96	1.00	1.00

NOTES.—The units are 0.01 TOT counts s^{-1} $(4.5\ deg^2)^{-1} \approx 1.54 \times 10^{-10}$ ergs s^{-1} cm^{-2} sr^{-1}. The parameter a_1 corresponds to the intensity of the XRB, a_2 is emission from the LSC, a_3 is detector drift, a_4 is Galactic secant-law emission, and a_5 is emission proportional to the Haslam map [in units of 0.01 TOT counts s^{-1} $(4.5\ deg^2)^{-1}$ K^{-1}]. σ_a is the error in the fit for photon counting noise only, σ_b includes fluctuations in the XRB modeled as the dashed curve in Fig. 2, and σ_c includes fluctuations modeled as the solid curve of Fig. 2.

the flux associated with the supercluster is positive by 2.9 and 2.3 σ in maps 1 and 2 even when the fluctuations in the XRB are taken into account. If the noise is Gaussian then the levels of significance of these two fits are 99.8% and 99%, respectively. The residuals to the fit to map 2 are indistinguishable from Gaussian even at the extremes (~ 4 σ) of the distribution, while the residuals to the fit to map 1 display a non-Gaussian tail for values larger than $+2$ σ. Approximately 1.5% of the pixels fall in the non-Gaussian portion of the tail. This is presumably due to inadequate windowing of sources. An independent test for statistical significance is discussed in § 4.4 and indicates that the result of the fit to map 2 is, indeed, significant at the 99% level, while the fit to map 1 is somewhat less significant.

An equivalent way of expressing the significance of the fits is to compute the change in χ^2 when the parameter associated with supercluster emission is removed from the fit. In the case of the fit to map 2, χ^2 increases by $\Delta\chi^2 = 36.5$. If one then takes into account the reduction in the degrees of freedom due to the PSF and clustering of sources, this value must be reduced by a factor of 6.8, i.e., an effective change in χ^2 of $\Delta\chi^2_{\rm eff} = 5.3$. This corresponds to a 2.3 σ level of significance as expected. A similar situation holds for the fit to map 1.

Taken at face value, the fits in Table 1 indicate the presence of diffuse X-ray emission in the plane of the local supercluster. However, a great many checks must be made on the robustness of this result: e.g., whether or not the signal comes from a few strong point sources located near the supergalactic plane; whether or not the signal is due to X-ray emitting galaxies distributed in the LSC; whether or not the signal arises from a chance alignment of fluctuations in the X-ray background; whether or not the result is sensitive to the pillbox model parameters; etc. The next section contains a detailed discussion of these issues.

TABLE 2

CORRELATION COEFFICIENTS FOR THE FIT PARAMETERS FOR MAP 1 IN TABLE 1

Fit Parameter	a_1	a_2	a_3	a_4	a_5
a_1	1.0	−0.4	−0.1	−0.5	−0.5
a_2	−0.4	1.0	0.0	0.2	0.0
a_3	−0.1	0.0	1.0	−0.3	0.0
a_4	−0.5	0.2	−0.3	1.0	−0.3
a_5	−0.5	0.0	0.0	−0.3	1.0

NOTES.—The fit parameters, a_k, are defined as in Table 1. The coefficients for map 2 are similar.

While photon counting noise is smaller than intrinsic sky fluctuations, it is not negligible and, furthermore, varies by a factor of 2 over the sky. The resulting total variance, shot noise plus sky fluctuations, varies by $\sim \pm 20\%$ from the mean. One might argue that it is better to weight the individual terms in χ^2 (see eq. [2]) inversely with the total variance appropriate for each pixel. Certainly this should reduce somewhat the error in the fit. If the analyses are performed in this way, the fits for the local supercluster parameter, a_2, decrease by an average of about 4% while the errors in the fits decrease by an average of about 2%; i.e., the results are not significantly different. We prefer to weight the pixels equally to minimize any systematic structure in the map that happens to be correlated with the pattern of nonuniform sky coverage.

4. SYSTEMATICS

4.1. *The Galaxy*

Even though the plane of the Galaxy, a strong source of X-ray emission, was removed from the map (see § 2), high Galactic latitude emission is large enough to be a potential source of error. However, the planes of the Galaxy and the LSC are nearly perpendicular and the center of the LSC is nearly at the Galactic pole. It is these fortuitous circumstances that result in nearly uncorrelated Galaxy and LSC fit parameters (see Table 2). As a consequence, one expects that the fit to LSC emission will be nearly independent of Galactic emission. As an alternative Galaxy model, we considered the two disk, exponentially truncated model of Iwan et al. (1982). The χ^2 for the fits with this model were slightly worse while the LSC fit parameters were essentially unchanged ($\delta a_2 \lesssim 3\%$). Even if the Galaxy model is left out of the fit entirely, the resulting LSC emission is reduced by only $\sim 21\%$; however, the χ^2 is significantly worse, $\Delta\chi^2_{\rm eff} = 11$. Therefore, we consider it unlikely that the supercluster emission found above is due to Galaxy contamination.

4.2. *Compton-Getting Dipole*

As discussed in § 2, the X-ray map was corrected for the Earth's motion relative to the average rest frame of the distant universe as defined by the CMB dipole. This is justi-

fied since the bulk of the X-ray background arises from sources at high redshift ($z \gtrsim 1$). The amplitude of the X-ray dipole is easily computed from the CMB dipole and the spectrum of the X-ray background, i.e., $\delta I_X/I_X = 4.3 \times 10^{-3}$, which is ~ 3.4 times larger than the CMB dipole. In addition, it is likely that X-rays trace the asymmetric mass distribution that created our peculiar velocity, and one would expect an intrinsic dipole moment in the XRB that is more or less aligned with the Compton-Getting dipole. However, it seems unlikely that the former will be as large as the latter. From unified models of the XRB (e.g., Comastri et al. 1995), less than 0.2% of the XRB background arises from sources within 50 Mpc and with fluxes $< 3 \times 10^{-11}$ ergs s^{-1} cm^{-2}. Lahav et al. (1997) demonstrated that the large-scale structure dipole can be comparable to the Compton-Getting dipole if one assumes, contrary to observations, unevolving X-ray luminosity and no upper limit on source flux. It is unlikely that their calculation is relevant to our analysis; nevertheless, we considered the possibility that the dipole correction made to the data is in error. If a dipole term is included in the fit, it is also not strongly correlated with the "pillbox" term and the resulting LSC emission increases by $\sim 15\%$ for map 1 and decreases by only $\sim 5\%$ for map 2. The χ^2 were only marginally better ($\Delta\chi^2_{\rm eff} \sim -1$) if these terms are included. It is interesting that the resulting fitted dipoles for the two maps agree within errors with that predicted for the Compton-Getting dipole. For map 2, the fitted dipole amplitude is $\delta I_X/I_X = 5.3 \pm 1.8 \times 10^{-3}$ while the direction is $\sim 19°$ from the CMB dipole, which is well within the directional error. For map 1 these values are $\delta I_X/I_X = 2.7 \pm 1.8 \times 10^{-3}$ and $\sim 35°$, also consistent with the Compton-Getting dipole. We find the results of the dipole fits significant in that they indicate that large-scale structure can be detected at this level. If the dipole term is excluded altogether from the fit, the values of LSC emission for the two maps increase by about 30%.

4.3. *Time Drift*

The time drift fit parameter in Table 1 corresponds to somewhat less than 2% of the XRB during the six month interval of the observations and, therefore, is also of potential concern. However, from Table 2 it is evident that this fit parameter is essentially uncorrelated with the LSC parameter indicating that our estimate of LSC emission is also not very sensitive to drift of detector sensitivity. In the case that the linear time drift model is removed from the fit, the LSC parameter is unchanged for map 2 and decreases by only 2% for map 1, while the χ^2 are significantly worse in both cases, i.e., $\Delta\chi^2_{\rm eff} = 24$ and 32 for the two fits, respectively. In order to test the limitations of the linear time drift model we included cubic and quadratic terms as well. The solutions and χ^2 were essentially unchanged. We conclude that detector drift cannot account for the observed emission from the LSC.

The Galaxy, the dipole, and the effects of time drift are all more or less orthogonal to the LSC. In fact, if we remove all three of these items from the analysis, the fit to LSC emission decreases by only 4% for map 2 and by 20% for map 1, while, of course, the χ^2 are much worse.

4.4. *The XRB*

It is now generally accepted that the X-ray background is composed of discrete sources (Hasinger et al. 1993; Georgantopoulos et al. 1997). Source confusion due to the finite resolution of the map along with inherent clustering of sources results in fluctuations in the XRB with an angular scale of about 3° and an amplitude of about 3% of the background. On the other hand, the implied LSC emission is about 1% of the XRB, so it is important to consider whether or not chance alignments of these fluctuation could account for it.

To the extent that fluctuations in the XRB can be modeled as in § 3.5, the above analysis indicates that the fit to LSC emission is significant at the 2.3–2.9 σ level. As an independent check, we repeated the fits for 5000 pillbox models with a uniform distribution of orientations in the sky. Because of the extensive windowing of the Galactic plane, models lying within 30° of the Galactic plane were disregarded. Also because of the "detected" LSC emission, models lying within 30° of the LSC plane were also excluded. For map 1, the amplitude of LSC emission in Table 1 exceeds those of 97% of the trials, while 93% of the χ^2 of the trial fits exceed the value in the table. Only 2.6% of the trials have LSC emission greater and χ^2 less than those listed in Table 1. The results for map 2 are even stronger. The LSC emission exceeds the fits of 99% of the trials, while the χ^2 is exceeded by 97% of the χ^2 of the trials. Only 0.7% of the trials have LSC emission greater and χ^2 less than the values listed in Table 1. If one includes the models that lie within 30° of the plane of the LSC, the results for map 2 are essentially the same, while for map 1 4.6% of the trials have LSC emission greater and χ^2 less that those listed in Table 1. Map 1 has significantly more "hot spots" than the more heavily windowed map 2, as is evidenced by the non-Gaussian tail mentioned in § 3.5 above. It is perhaps not surprising that map 1 is more susceptible to chance alignments of these sources, resulting in spuriously large amplitudes of emission associated with several pillbox models. On the other hand, the residuals of the fit to map 2 are Gaussian distributed, and an accidental 2.3 σ positive signal can be expected to occur in 1% of the trials. That this agrees with the level of occurrence in the rotated fits is an indication that the noise is well characterized; however, the exact agreement is probably fortuitous. We conclude that, at the $\sim 99\%$ confidence level, fluctuations in the XRB are not responsible for the observed signal.

4.5. *Pillbox Model*

The pillbox model for the LSC is highly simplistic; however, more refined models seem unwarranted considering the relatively low signal-to-noise ratio ($< 3\ \sigma$) indicated in Table 1. Nevertheless, several important checks of the model can be made. The checks illustrated in the figures below are for the more extensively windowed map 2; however, the conclusions are essentially the same for both maps.

Figure 3 is a plot of the LSC emission fit for a series of pillbox models lying in the supergalactic plane but with centers rotated by angles in steps of 30° from the nominal center of the LSC in Virgo. It is clear that the largest emission signals occur when the model center is near the nominal direction. In addition, the χ^2 of the fits are significantly worse for models rotated by angles $\geq 60°$. The lowest χ^2 occurs (for both windowed maps) at an angle of $-23°$ for which the LSC emission is somewhat larger; however, the differences from the Virgo-centered model are not significant.

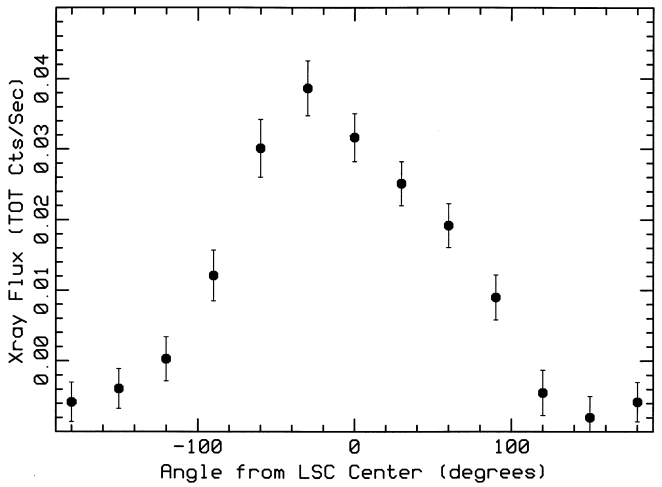

FIG. 3.—LSC emission fitted to map 2 for pillbox models lying in the supergalactic plane with centers rotated by angles in steps of 30° from the nominal center of the LSC in Virgo. The error bars are statistical only and are highly correlated. The units are TOT counts s^{-1} $(4.5\ \mathrm{deg}^2)^{-1} \approx 1.54 \times 10^{-8}\ \mathrm{ergs\ s^{-1}\ cm^{-2}\ sr^{-1}}$.

The dependence of the results on the vertical position of the Galaxy within the disk of the LSC is illustrated in Figure 4. The vertical position is expressed in terms of the disk thickness, H_{SC}, so ± 0.5 represents the top and bottom of the disk. Again the nominal central position yields the largest LSC emission with the χ^2 of the fits increasing significantly at the extremes.

Figure 5 illustrates the dependence of results on the radial position of the Galaxy in the LSC. Position is expressed in units of the supercluster radius. The nominal value is 0.8. It is clear from the figure that the largest LSC emission is found for models with the Galaxy near the edge of the LSC (note: negative values indicate models with centers in the direction opposite Virgo). The model with the nominal radial position has the smallest value of χ^2, while models with radial positions ≤ 0.5 have significantly larger χ^2. For this test the results for map 1 differ somewhat in that models with radial positions ≥ 0.2 have reasonable χ^2; however, the fitted LSC emission is comparable for all these models.

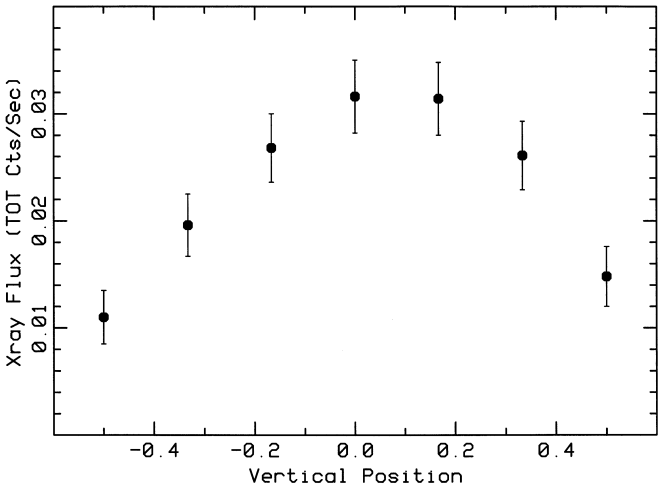

FIG. 4.—LSC emission fitted to map 2 for pillbox models with central planes offset from the Galaxy. Vertical position is expressed in terms of the thickness of the pillbox. The error bars are statistical only and are highly correlated. The units are the same as in Fig. 3.

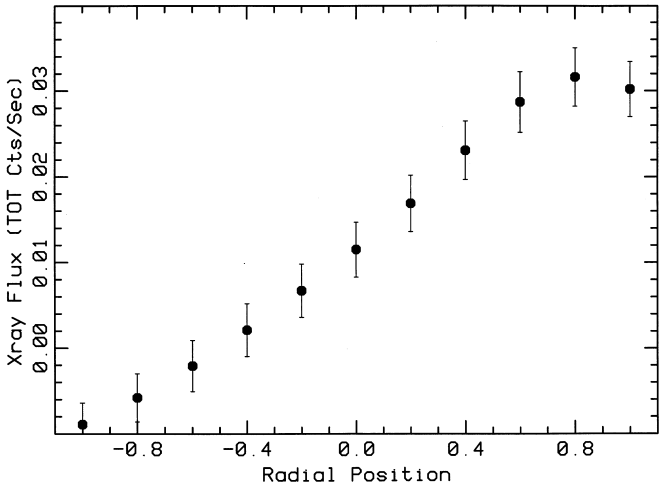

FIG. 5.—LSC emission fitted to map 2 for pillbox models with centers displaced from the Galaxy. Radial position is expressed in units of the supercluster radius. The nominal value is 0.8. Negative values indicate models with centers in the direction opposite Virgo. The error bars are statistical only and are highly correlated. The units are the same as in Fig. 3.

In order to test specifically whether or not a few isolated hot spots in the supergalactic plane are responsible for the signal, the data are binned according to that emission predicted from the pillbox model and then plotted in Figure 6 as a function of emission predicted from the model. The scale of the predicted emission is taken from Table 1, and the data are corrected for all fitted large-scale structure except for LSC emission. If the signal is due to hot spots in the direction of the center of the LSC, the extreme right hand data point would fall well above the unity slope curve, while other points would fall well below the curve. Within the limitations of the signal-to-noise ratio, it appears that this is not the case. Of course, the disposition of the data is sensitive to the binning. While finer scale binning does show a great deal of scatter, the linear trend is clear. The data from map 1 show the same trend with a bit more scatter.

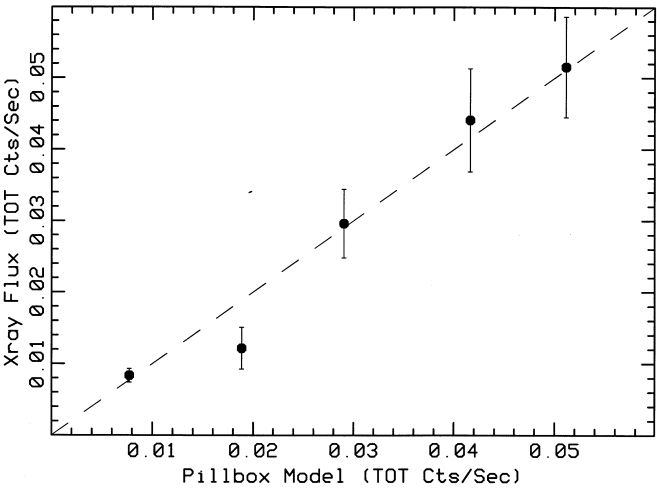

FIG. 6.—Average 2–10 keV flux of map 2 binned according to level of emission predicted from the pillbox model. The predicted emission is taken from Table 1, and the map is corrected for all fitted large-scale structure except for LSC emission. The error bars are statistical only. The units are the same as in Fig. 3.

Finally we investigated how sensitive the results are to varying the thickness to diameter ratio of the pillbox model. The answer is, "not very." For map 1, only for ratios H_{SC}/D_{SC} less than 1/12 and greater than 1/4 are the χ^2 of the fits significantly worse. For map 2 these values are 1/16 and 1/2. The values of LSC emission decrease somewhat as H_{SC}/D_{SC} increases; however, the statistical significance of detection is roughly the same for all models in this range. One can deduce only a very rough value of the thickness to diameter ratio from the data and must rely on the optical structure of the LSC (Tully 1982). Clearly, the more important aspect of the models is that the emission is enhanced in the general direction of Virgo.

4.6. *Windowing*

As discussed in § 2, pixels of the X-ray map were flagged if they were (1) too close to the plane of the Galaxy, (2) near strong X-ray sources, or (3) near positive fluctuations in the XRB. Failing to remove the strong X-ray sources results in a very poor fit with a reduced χ^2 of $\chi^2_\nu = 13$. Therefore, these cuts are absolutely necessary. On the other hand, the results of § 3.5 are relatively insensitive to the other two cuts. The level of LSC emission changes by less than 30% if the Galactic plane cut is varied between 20° and 50° (the smallest fitted value of LSC emission is only 5% less than that of Table 1). Similarly, the fitted LSC emission does not change significantly from the minimally windowed map 1 to a map with only 20% full sky coverage.

4.7. *X-Ray Autocorrelation Function*

As a check on how well the modeled structure matches the X-ray sky, the autocorrelation function (ACF) of the map was compared with that predicted by the model. One might expect that the unity values of the χ^2 of Table 1 indicate that the fit is quite good. However, recall that this value was forced by assuming that all the excess variance was due to fluctuations in the XRB. If the excess were due to unmodeled large-scale structure, then the modeled ACF would not fit the data. Figure 7 shows that the ACF is reasonably well modeled and that there appears to be little other large-scale structure in the map. The solid curve of Figure 2 was taken as the model of the small-scale fluctuations in the XRB. For $\theta > 10°$ the data are binned in 13° bins to reduce scatter.

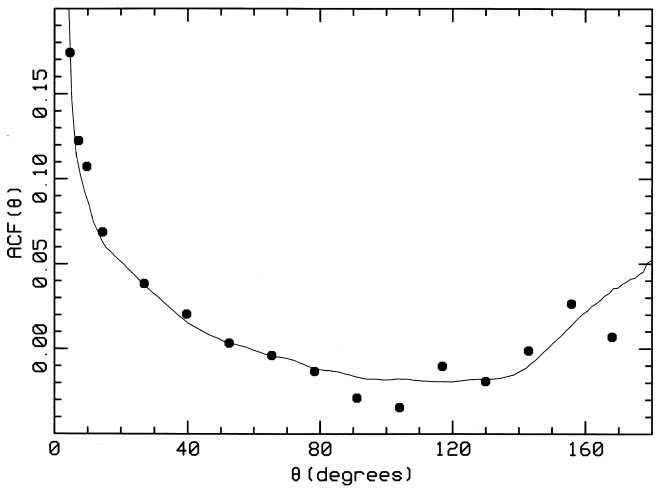

FIG. 7.—Autocorrelation function (normalized to unity) of map 2. For $\theta > 10°$ the data are binned in 13° bins to reduce scatter. The solid curve is the ACF for the model including all fitted large-scale structure plus the fit of Fig. 2 for the small-scale ($< 10°$) structure.

4.8. *Point Sources*

Even if the above arguments indicate that there is X-ray emission associated with the plane of the LSC, it is not at all clear that this emission originates from diffuse gas. After all, there are a great many galaxies and several clusters in this plane, and all of these emit X-rays at some level. However, there are several indications that it is not the case that individual sources contribute significantly to the X-ray emission in the LSC plane. At a distance of 20 Mpc, the cutoff flux of the present map (3×10^{-11} ergs s^{-1} cm^{-2}) corresponds to a luminosity of $\sim 10^{42}$ ergs s^{-1}; therefore, only relatively weak (compared to AGNs) sources could contribute. The observed upper limit of the average 2–10 keV emissivity of such sources in the local ($z \lesssim 0.1$) universe is $4 \times 10^{38}\ h$ ergs s^{-1} Mpc^{-3} (Miyaji et al. 1994), where h is the Hubble constant in units of 100 km s^{-1} Mpc^{-1}. On the other hand the pillbox model of the LSC and the amplitude of the X-ray flux in Table 1 imply an average X-ray emissivity of $3.0 \times 10^{39}(R_{SC}/20\ \mathrm{Mpc})^{-1}$ ergs s^{-1} Mpc^{-3} (see § 6). Thus for a Hubble constant of 60 km s^{-1} Mpc^{-1} the ratio of the observed LSC emissivity to the average emissivity of weak sources is $\gtrsim 12$. For an LSC collapse factor of ~ 10, the observed emissivity could be due to weak sources without seriously violating this constraint.

However, unified models of the XRB indicate that it is unlikely that weak sources make a significant contribution to the average X-ray emissivity. For example, the model of Comastri et al. (1995) implies an average, local 2–10 keV emissivity of $7.6 \times 10^{38}\ h$ ergs s^{-1} Mpc^{-3}, which is consistent with the observed value ($8.6 \pm 2.4 \times 10^{38}\ h$ ergs s^{-1} Mpc^{-3}) derived by Miyaji et al. (1994) from a cross-correlation analysis of the *HEAO 1* A2 map with galaxies from the *IRAS* survey. The Comastri model (by design) accounts for the entire XRB. According to this model, weak sources make only a small contribution to the local emissivity, i.e., $< 7.6 \times 10^{37}\ h$ ergs s^{-1} Mpc^{-3}. For $h = 0.6$ this is a factor of ~ 65 less than inferred for the LSC. If weak sources account for the LSC emissivity, then either Comastri et al. (1995) seriously underestimate their numbers or the LSC collapse factor is much larger than observed for visible galaxies. While the above argument is suggestive, it is based on a unified AGN model that is by no means certain. In fact, there is some speculation that weak sources do make a significant contribution to the XRB (Yi & Boughn 1998; Di Matteo & Fabian 1997). Stronger constraints on the point-source contribution to LSC emissivity come from the consideration of two source catalogs, the Nearby Galaxies Catalog (NBG; Tully 1988) and the *ROSAT* All-Sky Survey Bright Source Catalog (Voges et al. 1996).

There are 2367 galaxies in the NBG catalog, which consists of all galaxies with known velocities ≤ 3000 km s^{-1}. This catalog is dominated by two data sets: the Shapely-Ames sample and the all-sky survey of neutral hydrogen. Although the catalog has severe incompleteness problems at velocities above 2000 km s^{-1}, the coverage is homogeneous across the unobscured part of the sky (Tully 1988). In any case, if point X-ray sources associated with galaxies in the LSC are an important source of X-ray emissivity, it seems reasonable that much of the emission would be associated with the galaxies in this catalog. To check this

possibility, the X-ray map was further cleaned by removing ~ 15 deg^2 regions (somewhat larger than the PSF of the map) at the location of all of catalog galaxies. Many of these regions lie in already windowed sections of the map. After the additional cuts the sky coverage was reduced to 26% for map 1 and 18% for map 2. The reduced coverage results in an increase in noise; however, the levels of LSC emission are still marginally significant (2 σ and 1.5 σ for map 1 and map 2, respectively) and are somewhat larger than but consistent with the values in Table 1.

Another check of the level of contribution of galaxies from the NBG catalog was made by fitting the LSC pillbox plus a monopole to the 15 deg^2 regions surrounding the galaxies but with the appropriate windowing of maps 1 and 2. Before the fits, the maps were corrected for a dipole, the Galaxy, and instrumental drift. The sky coverage for these fits was only 21% and 15%; however, if these regions dominate LSC emission, then the amplitude of the fit should be considerably larger than in Table 1. This was not the case. In fact, the fit amplitudes of LSC emission are essentially the same as those in Table 1. Although the above tests are consistent with diffuse LSC emission, the Tully galaxies (smoothed by the PSF) occupy a great deal of the LSC plane, so this conclusion must be tempered.

One final check on the galaxy contribution was to generate a map by assigning an X-ray flux to each galaxy, convolve the resulting map with the PSF, and then apply the windowing appropriate for maps 1 and 2. The X-ray flux of the galaxies was obtained by cross-correlating the X-ray map with an appropriately smoothed map of galaxy number density. This was done in four different distance bins (0–10, 10–20, 20–30, and 30–50 Mpc) in order to account for distance dependence of flux. Only for the first bin was the correlation statistically significant. The X-ray emission from galaxies was determined using the 1 σ upper limits of the cross-correlation for the appropriate distance bin. The linear regression applied to the resulting maps yields upper limits to LSC emission that are a factor of 3 below the levels of Table 1. This result is another indication that X-ray emission from galaxies is not the major component of X-ray emission from the LSC plane.

A more direct indication of the contribution of point sources is the *ROSAT* All-Sky Survey (RASS) Bright Source Catalog (Voges et al. 1996). There are 18,811 sources in this catalog down to a 0.1–2.4 keV flux limit of 0.05 counts s^{-1} (3×10^{-13} ergs s^{-1} cm^{-2} for a photon spectral index of $\alpha = -2$, where $dN/dE \propto E^{\alpha}$). At a brightness limit of 0.1 counts s^{-1} (8547 sources) the catalogue represents a sky coverage of 92%. Two hardness ratios, HR1 and HR2, are defined by HR1 $= (B - A)/(B + A)$ and HR2 $= (D - C)/(D + C)$, where A, B, C, and D are the count rates in passbands that correspond roughly to 0.1–0.4, 0.5–2.0, 0.5–0.9, and 0.9–2.0 keV (Snowden et al. 1995). The average HR2 hardness ratio of the sources corresponds to a photon spectral index of $\alpha \sim -2$, although there are certainly sources that are much harder as well as sources that are much softer than this spectrum. For $\alpha = -2$, the catalog limit corresponds to a 2–10 keV flux of 2×10^{-13} ergs s^{-1} cm^{-2}, which is about 2 orders of magnitude below the Piccinotti et al. (1982) sources (see § 2). If there is a significant population of relatively faint (3×10^{-13} to 3×10^{-11} ergs s^{-1} cm^{-2}) sources in the LSC, then a large fraction of these should show up in the Bright Source Survey. Even though the completeness level is not entirely uniform, the catalog can still be used to give an indication of the level of contamination by point sources. There are too many RASS sources to simply window them from the *HEAO* map (3° cuts around each source would window the entire map); however, there are several ways of testing for the effects of RASS point sources.

To check the contamination due to relatively bright sources or clusters of sources, we constructed a B-band (0.5–2.0 keV) map of RASS sources convolved with the *HEAO* PSF. If the resulting B-band flux in any pixel was greater than 0.1 counts s^{-1} (for $\alpha = -2$, this corresponds to a flux of 1×10^{-12} ergs s^{-1} cm^{-2}), then a 15 deg^2 region about the pixel was windowed from the two previously windowed *HEAO* maps, i.e., maps 1 and 2. Note that a single source with a flux of 0.9 counts s^{-1} is at the cutoff flux after smoothing with the PSF. The resulting heavily windowed maps, map 1′ and map 2′, had sky coverages of 22% and 17%, respectively. When the linear regression of § 3.4 was performed on these two maps, the fits to LSC emission were somewhat larger but not significantly different than the fits of Table 1. The errors in the fits were about 50% larger because of the reduced sky coverage. Similar results were obtained when the RASS cutoff flux level was varied as well as for windowing individual sources (i.e., not convolved with the PSF) with B-band fluxes above a cut-off level. These results indicate that the LSC emission indicated in Table 1 is not due to the brighter of the RASS sources.

As another check on contamination, every source in the RASS catalog was assigned a 2–10 keV flux from its B-band flux by assuming a spectral index of $-1 < \alpha < -3$, which was deduced from HR2 hardness ratio. For faint sources, the quantity HR2 is quite noisy and the computed value of α might be either larger than -1 or smaller than -3. For these sources α was simply forced to be -1 or -3, which we consider to the limits of the range for nearly all X-ray sources. The B-band fluxes were corrected for Galactic extinction using H I column density maps (Stark et al. 1992; Dickey & Lockman 1990) and the absorption coefficients of Morrison & McCammon (1983). These corrections made little difference and, in any case, are probably less important than internal extinction in the sources themselves. The resulting 2–10 keV flux map was then convolved with the *HEAO* PSF and subtracted from the *HEAO* maps, map 1 and map 2. The linear regressions applied to these corrected maps implied LSC emission somewhat larger than but not significantly different from the values in Table 1.

As an upper limit to the contamination by RASS sources, we applied the above map correction assuming that every source has a very hard spectrum, i.e., $\alpha = -1$. The linear regression fit to map 2 was essentially unchanged, while the LSC emission fit to map 1 was reduced by about 40%. Assuming that every source has the average spectral index, i.e., $\alpha = -2$, yields results that are virtually indistinguishable from those of Table 1.

At the catalog limit, 0.05 counts s^{-1}, the coverage is probably less uniform than at a limit of 0.1 counts s^{-1}; therefore, we repeated the above corrections for the brightest 8547 RASS sources (>0.1 counts s^{-1}). The results were virtually unchanged.

Because of the effects of nonuniform coverage and imperfect knowledge of the spectra of individual sources, the above source corrections to the 2–10 keV flux are not particularly accurate. On the other hand, they do indicate that the emissivity of weak X-ray sources in the LSC is at least

an order of magnitude less that those implied in Table 1, and we conclude that those results are not contaminated by point sources.

4.9. *Clusters of Galaxies and the Great Attractor*

It is well known that rich clusters of galaxies are strong X-ray emitters and, therefore, are a potential source of contamination. Distant clusters are indistinguishable from the point sources discussed above. In addition, 30 bright, nearby clusters including Virgo, Coma, and Centaurus are among the Piccinotti et al. (1982) sources and have already been windowed from the map. However, extended emission associated with nearby less compact clusters of galaxies might be considered a possible source of contamination.

Ebeling et al. (1997) used the *ROSAT* Brightest Cluster sample to fit a Schechter luminosity function to clusters and obtained a 2–10 keV L^* of 1.2×10^{45} ergs s^{-1} and a power-law exponent of -1.51. Using these values, the implied total 2–10 keV emissivity is $\varepsilon_X = 1.3 \times 10^{38}$ ergs s^{-1} Mpc^{-3}, which is a factor of 25 less than that implied by the values of Table 1 (see § 6). On the other hand, the luminosity of the Virgo cluster is $\sim 1.4 \times 10^{43}$ ergs s^{-1}, and sources this bright would be cut from the windowed data if they were within 60 Mpc. Again using the fit of Ebeling et al. (1997), the total emissivity of clusters less luminous than the Virgo cluster is $\varepsilon_X = 1.6 \times 10^{37}$ ergs s^{-1} Mpc^{-3} or a factor of 200 less than the implied LSC emissivity. Even if this flux is increased by the collapse factor of 10, it is still considerably less than that inferred for the LSC (see § 6).

As a further check on possible contamination by extended emission from galaxy clusters, we extended the windowing of the X-ray map to include 15° diameter regions around the Virgo, Centaurus, Coma, Fornax, and Ursa Major clusters as well as around the most dense regions of the Hydra, Pavo, Perseus, and Ophiuchus galaxy clouds (Tully 1988). Finally the diffuse emission found by Jahoda & Mushotzky (1989) was eliminated by windowing a 40° diameter region about the Great Attractor. Fits of the LSC emission to these further windowed maps were only $\sim 15\%$ less that those of Table 1, while the errors in the fit were, of course, somewhat larger. Therefore, there is no indication that the fits of Table 1 are contaminated by either the cores of clusters of galaxies or by diffuse emission from the Great Attractor.

The windowing of more extensive regions of galaxy clouds in the LSC would not be possible without cutting most of the plane of the LSC, and, in any case, it is not clear that one should distinguish such emission with diffuse emission in the LSC. This point is essentially the same as asking whether LSC emission is smooth or somewhat clumpy and will be addressed in § 6 below; however, the bottom line is that the signal-to-noise ratio is simply not high enough to be able to give a clear answer.

5. SUNYAEV-ZELDOVICH EFFECT IN THE LSC

If the diffuse X-ray emission in the LSC is due to Bremsstrahlung from a hot, ionized intergalactic medium, then one might expect its signature to be imprinted upon the cosmic microwave background (CMB) via inverse Compton scattering, i.e., the Sunyaev-Zeldovich (SZ) effect (Sunyaev & Zeldovich 1980). If the gas were uniformly distributed, the profile in the CMB would be the same as in the X-ray except with a negative amplitude for observations on the Rayleigh-Jeans side of the blackbody spectrum. The CMB temperature decrement for radiation passing through a gas cloud of uniform electron density N_e, thickness L, and temperature T_e is given by (e.g., Hogan 1992)

$$(\delta T/T)_{\rm CMB} \approx 4.0 \times 10^{-6} \beta l n_e t_e \,, \tag{5}$$

where $l = L/10$ Mpc, $n_e = N_e/10^{-5}$ cm^{-3}, $t_e = kT_e/10$ keV, $\beta = [x(e^x + 1)/(e^x - 1) - 4]$, and $x = h\nu/kT_{\rm CMB}$. For $L = 20$ Mpc, $N_e = 2.5 \times 10^{-6}$, and $kT_e = 10$ keV, the Rayleigh-Jeans decrement in the CMB is $|\delta T/T| \sim 4 \times 10^{-6}$. This value is somewhat smaller than the 10° scale fluctuations observed by the *COBE* DMR experiment, comparable to other large-scale structure in the microwave sky, e.g., high-latitude Galactic emission and the expected intrinsic CMB quadrupole, and only marginally larger than the instrument noise in the DMR data (Bennett et al. 1996). Nevertheless, we performed the same type of analysis as for the X-ray background described in § 3 above.

The four year 53 GHz DMR map was obtained from the *COBE* data archive in $2\overset{\circ}{.}6 \times 2\overset{\circ}{.}6$, ecliptic, quadrilaterized spherical cube projection format (Bennett et al. 1996). This map was deemed more appropriate than the 31 GHz or 90 GHz maps because of a combination of low instrument noise, low Galaxy background, and moderately large β (see eq. [5]). An 11 parameter linear regression similar to that of § 3.4 was performed on the map after flagging all pixels within 20° of the Galactic plane and within 30° of the Galactic center. The fit parameters were a monopole, a dipole, a quadrupole, a secant-law Galaxy model, and the amplitude of the canonical pillbox model of the LSC. As with the *HEAO* X-ray map, the sky coverage for the DMR maps and, hence, instrument noise are not uniform across the sky. In this case the instrument noise per pixel is larger than the intrinsic sky fluctuations, so the contribution to χ^2 (see eq. [2]) of each pixel is weighted inversely with the noise variance of the pixel. However, the results did not change significantly when the analysis was repeated with equally weighted pixels. The formal fit to the pillbox amplitude (normalized to $1R_{\rm SC}$) is

$$\delta T_{\rm CMB} = -17 \pm 5 \ \mu{\rm K} \,, \tag{6}$$

where the uncertainty is statistical only and assumes uncorrelated instrument noise.

As mentioned above, this level is comparable to other systematic structure in the map and, therefore, should by no means be considered as a 3 σ detection. As an estimate of the significance of the result, the analysis was repeated for 5000 model pillboxes with a uniform distribution of orientations in the sky. As in § 4.4 models lying within 30° of the Galactic and supergalactic planes were disregarded. The amplitude of the SZ effect of equation (6) is more negative than 82% of the rotated models, indicating a significance of ~ 1 σ. On the other hand, 80% of the χ^2 of the trial fits exceed that of the fit of equation (6) and 9% of the trials have more negative SZ fits and smaller χ^2 than the LSC model. If one includes models that lie within 30° of the plane of the LSC, these results do not change significantly. Nor are they changed for analyses in which the pixels are weighted equally.

Because of the low level of the signal, only a few checks for systematics were made. The method of § 4.5 was used to exclude the possibility that a single "hot" or "cold" source accounted for the signal. The LMC, SMC, and Orion Nebula were explicitly excluded with no significant change in the fit. Finally the three DMR maps (31, 53, and 90 GHz)

were combined according to the prescriptions suggested by Hinshaw et al. (1996) to minimize the effect of the Galaxy. These combinations have larger effective noise and so result in larger statistical errors for the fits of the pillbox amplitude. The fit amplitudes varied from -5 μK to -22 μK. While it is clear the SZ effect due to hot gas in the LSC is not significantly detected, we note that the upper limit is consistent with the amount of hot, diffuse gas required to account for the diffuse X-ray emission discussed in § 6. We do find it intriguing that the fits correspond to a decrement in the CMB as predicted by the SZ effect.

6. DISCUSSION

If one takes seriously the hypothesis that hot, diffuse gas in the LSC is responsible for the diffuse X-ray emission claimed in § 3, then the strength of the emission can be used to constrain the density and temperature of the gas. For simplicity assume a uniform, isothermal gas with electron temperature T_e and electron density N_e. Then the 2–10 keV X-ray intensity due to Bremsstrahlung is given by (e.g., Rybicki & Lightman 1979, p. 159)

$$I_{\rm X} = \varepsilon_{\rm X} L/4\pi = 4.0 \times 10^{-9} n_e^2 t_e^{1/2} l \text{ ergs s}^{-1} \text{ cm}^{-2} \text{ sr}^{-1} , \quad (7)$$

where L is the thickness of the emitting region, $l = L/10$ Mpc, $n_e = N_e/10^{-5}$ cm^{-3}, and $t_e = kT_e/10$ keV. Primordial element abundances are assumed; however, the coefficient in equation (7) increases by only a factor of 1.14 for solar abundance. From Table 1, the amplitude of the LSC emission normalized to $1R_{\rm SC}$ is $\sim 3.3 \times 10^{-2}$ TOT counts s^{-1} (4.5 deg^2)$^{-1}$, which corresponds for a 10 keV Bremsstrahlung spectrum to

$$I_{\rm X} = 5.0 \times 10^{-10} \text{ ergs s}^{-1} \text{ cm}^{-2} \text{ sr}^{-1} . \quad (8)$$

From equations (7) and (8) (with $L = R_{\rm SC}$),

$$N_e = 2.5 \times 10^{-6} (R_{\rm SC}/20 \text{ Mpc})^{-1/2} (kT_e/10 \text{ keV})^{-1/4} \text{ cm}^{-3} . \quad (9)$$

The implied gas density is only weakly dependent on $R_{\rm SC}$ and T_e. Moreover, it is reasonable to assume that $R_{\rm SC} \sim 20$ Mpc (roughly the distance to the Virgo cluster) and that $kT_e \sim 10$ keV. A temperature much greater than 10 keV would exceed the virial temperature of the LSC, while a temperature much less than 10 keV would have rendered the gas undetectable by *HEAO*. As a rough consistency check, the X-ray data were split into "soft" (2–5 keV) and "hard" (5–10 keV) components (Allen et al. 1994), and the "pillbox" fits of § 3 were repeated on the subdivided data sets. The ratio of the fit amplitudes (in counts s^{-1}) in these two bands is $\dot{N}_{\rm soft}/\dot{N}_{\rm hard} \lesssim 1$. Although the uncertainty in this ratio is considerable, it is consistent with an electron temperature of $\gtrsim 10$ keV but inconsistent with temperatures < 3 keV. Therefore, it seems unlikely that the implied electron number density could be much different than $N_e \sim 2$–3×10^{-6}. It is interesting to note that this value is roughly an order of magnitude larger than the mean number density of baryons in the universe and is consistent with a collapse factor of 10, which is roughly the aspect ratio of the LSC.

If this hot gas were distributed uniformly within a 40 Mpc diameter by 5 Mpc thickness supercluster, the implied total mass is $\sim 4 \times 10^{14}$ $M_\odot$. From dynamical considerations, Shaya, Peebles, & Tully (1995) have estimated that the total mass within a distance of 40 Mpc (about 40 times the volume of the LSC) is about 7×10^{15} $M_\odot$. On the other hand, the total mass in stars in the same volume is about 1×10^{14} $M_\odot$, which is an order of magnitude too small to account for the baryonic matter that should be present. While the mass of the hypothetical hot gas in the LSC is insufficient to account for the dynamical mass in the local universe, it may well make up the bulk of the baryonic matter.

These estimates rely on the gas being uniformly distributed. Since Bremsstrahlung is proportional to N_e^2, the emission is enhanced if there is any clumping of the gas. For example, if the gas is contained in 50% of the volume of the disk of the LSC, i.e., a clumping factor of 2, then the implied mean density decreases by a factor of $1/\sqrt{2}$.

As discussed in § 5 above, the presence of hot, ionized gas is imprinted via the SZ effect on the cosmic microwave background. For 10 keV gas with a density of 2.5×10^{-6} cm^{-3} and a thickness of 20 Mpc, the expected decrement in the CMB is ~ -11 μK for a Rayleigh-Jeans spectrum. While the fit of a pillbox LSC to the 53 GHz *COBE* map is consistent with this prediction, the systematic structure in the map is large and the agreement should be considered at best a 1 σ confirmation.

If superclusters (SCs) with hot gas are common in the universe, then their combined SZ effects would result in fluctuations in the CMB that might be confused with intrinsic CMB fluctuations (Hogan 1992). This has been demonstrated not to be the case for the *COBE* results (Boughn & Jahoda 1993; Bennett et al. 1993). To see how many SCs are allowed by this constraint, suppose that a fraction f of all baryonic matter is contained in SCs with diameters of 40 Mpc and thicknesses of 5 Mpc. Then the number density of SCs is $n_{\rm SC} = f/bV_{\rm SC}$, where $V_{\rm SC}$ is the volume of an SC and b is the collapse factor. If each results in a temperature decrement of $\delta T_{\rm CMB} \sim 2$ to 3 μK (for a path length equal to the thickness of the SC), then the rms fluctuations of a distribution of SCs should be $\sim 2.5 \times N_{\rm SC}^{1/2}$ μK, where $N_{\rm SC} \approx \pi R_{sc}^2 n_{\rm SC} r$ is the number of SCs along the line of sight out to a distance r. To compare with the *COBE* DMR data for which $\delta T_{\rm rms} \sim 35$ μK, we set $r \sim 400$ Mpc, at which a 40 Mpc SC would subtend an angle about equal to the *COBE* beam size. Even if $f = 1$, i.e., if all the baryons in the universe are in the form of hot, diffuse gas in SCs, the fluctuations caused by the SZ effect would be ~ 7 μK or about 1/5 the level of the CMB fluctuations. In all likelihood, the fraction f is much smaller than unity. From the supercluster (SC) catalog of Batuski & Burns (1985), Rephaeli (1993) estimated the local density of SCs to be 5×10^{-8} h^3 Mpc^{-3}. If these SCs have volumes and densities similar to that inferred for the LSC, then only about 0.001 of the baryonic matter in the universe is contained in SCs, i.e., $f = 0.001$. Then the SZ fluctuations would be quite small, $\lesssim 1$ μK. In any case, the spectrum of SZ fluctuations differs significantly from those intrinsic to the CMB.

Another way to detect the presence of the SZ effect is via a spectral distortion of the CMB that is quantified by the Compton y parameter, $y = \int (kT_e/m_e c^2) N_e \sigma_{\rm T} \, dl$, where T_e is the electron temperature, m_e is the electron mass, N_e is the electron density, $\sigma_{\rm T}$ is the Thompson scattering cross section, and l is the path length (e.g., Rephaeli 1993). Assuming an isothermal gas, this becomes $y = (kT_e/m_e c^2)\sigma_{\rm T} \int N_e \, dl$. A rough approximation of the integral is f times the mean baryon density times the Hubble radius,

i.e., $fn_b cH_0$. Then for $kT_e = 10$ keV, $y \sim 4 \times 10^{-5} f$. The limit on y from the *COBE* data is (Fixsen et al. 1996) $y \lesssim 10^{-5}$, which implies that $f \lesssim 1/4$. If $f \sim 0.001$, as inferred from the local density of SCs, then the presence of hot gas in these SCs is consistent with the upper limit to the spectral distortion of the CMB.

7. CONCLUSIONS

Evidence is presented in this paper for X-ray emission associated with the plane of the local supercluster (LSC); however, it should be emphasized that this emission is by no means firmly established. The two fits presented in Table 1 constitute only 2.9 and 2.3 σ results. Even though positive 3 σ detections have (Gaussian) confidence levels of 99.9%, such effects often warrant skepticism. This is usually due to uncertainty in the statistical properties of the noise and/or the lack of confidence that there are no unknown systematics. Indeed, it is known that the residual noise in the fit to map 1 has a small, although distinct, non-Gaussian tail that might well be the source of the relatively large number of "accidental" detections (3%) in the rotated data sets. However, the residual noise in the fit to map 2 is Gaussian, and, furthermore, the "accidental" detection level in the rotated data sets (1%) is consistent with that expected for a 2.3 σ effect. Therefore, we are reasonably confident that the 2.3 σ detection in map 2 is robust, i.e., that the 99% confidence level is appropriate. The fact that the fit to map 1 agrees with the fit to map 2 (as well as with those of even more aggressively windowed maps) gives us further confidence that non-Gaussian noise is probably not responsible for the effect.

X-ray emission from the plane of the LSC has been suggested previously (Jahoda 1993). We argue that, if the emission is at the level suggested by this paper, then it is unlikely to be produced by individual sources but rather is diffuse in nature. This would imply that there is a great deal of hot (~ 10 keV), diffuse ($\sim 2.5 \times 10^{-6}$ cm^{-3}) gas in the LSC and that the gas may account for the bulk of baryonic matter in the local universe. The presence of such gas would be imprinted on the cosmic microwave background (CMB) as a Sunyaev-Zeldovich temperature decrement of ~ -10 μK. While the *COBE* 53 GHz map is consistent with such structure, other systematics preclude the positive identification of this component. If superclusters are relatively plentiful in the universe and hot gas in them is common, the resulting fluctuations in the CMB would still be small relative to the those found in the *COBE* data and, therefore, unlikely to compromise the cosmological implications of those fluctuations.

Even if the presence of hot, diffuse gas in the LSC is not yet firmly established, the results presented here are tantalizing in that they are consistent with the density and temperature of gas that might be expected to inhabit the intergalactic medium. It is unlikely that more detailed analyses of the *HEAO* and *COBE* data will shed more light on the situation. The signal-to-noise ratios of these maps are simply not good enough. However, the next generation of X-ray satellites with higher angular resolution, better frequency resolution, and higher sensitivity will likely be able to either confirm or refute the suggestions made in this paper as well as be able to detect diffuse emission in other relatively nearby superclusters. Finally the new CMB satellites scheduled for launch in the next few years (i.e., the *Microwave Anisotropy Probe* [*MAP*] and *Planck*) should have the angular and frequency resolution required to distinguish an SZ effect in the LSC from intrinsic CMB fluctuations if the level of the effect is that suggested by this paper.

I would like to acknowledge Keith Jahoda, who is responsible for constructing the *HEAO 1* A2 X-ray map and who provided me with several data-handling programs. I would also like to acknowledge Ruth Daly, who initially suggested this project. Much of this work was completed at the Princeton University Gravitation and Cosmology computing cluster, where I benefited greatly from the subroutines of Ed Groth. Finally I would like to acknowledge the hospitality afforded me at the Institute for Advanced Study, where I collected many of my thoughts for this paper. This work was supported in part by NASA grant NAG 5-3015, the Monell Foundation, and (through Princeton University) NSF grant PHY-9222952.

REFERENCES

Allen, J., Jahoda, K., & Whitlock, L. 1994, Legacy, 5, 27
Anninos, P., & Norman, M. L. 1996, ApJ, 459, 12
Bahcall, N. A., & Soneira, R. M. 1984, ApJ, 277, 27
Banday, A. J., Gorski, K. M., Bennett, C. L., Hinshaw, G., Kogut, A., & Smoot, G. F. 1996, ApJ, 468, L85
Bardelli, S., Zucca, E., Malizia, A., Zamorani, G., Scaramella, R., & Vettolani, G. 1996, A&A, 305, 435
Batuski, D. J., & Burns, J. O. 1985, AJ, 90, 1413
Bennett, C. L., Hinshaw, G., Banday, A., Kogut, A., Wright, E. L., Lowenstein, K., & Cheng, E. S. 1993, ApJ, 414, L77
Bennett, C. L., et al. 1996, ApJ, 464, L1
Boldt, E. 1987, Phys. Rep., 146, 215
Boughn, S. P., & Jahoda, K. 1993, ApJ, 412, L1
Cen, R., & Ostriker, J. P. 1999, ApJ, 514, 1
Comastri, A., Setti, G., Zamorani, G., & Hasinger, G. 1995, A&A, 296, 1
Day, C. S. R., Fabian, A. C., Edge, A. C., & Raychaudhury, S. 1991, MNRAS, 252, 394
de Vaucouleurs, G. 1953, AJ, 58, 30
Dickey, J. M., & Lockman, F. J. 1990, ARA&A, 28, 215
Di Matteo, T., & Fabian, A. C. 1997, MNRAS, 286, 393
Ebeling, H., Edge, A. C., Fabian, A. C., Allen, S. W., Crawford, C. S., & Bohringer, H. 1997, ApJ, 479, 101
Einasto, M., Tago, E., Jaaniste, J., Einasto, J., & Andernach, H. 1997, A&AS, 123, 119
Fixsen, D. J., Cheng, E. S., Gales, J. M., Mather, J. C., Shafer, R. A., & Wright, E. L. 1996, ApJ, 473, 576
Georgantopoulos, I., Stewart, G. C., Blair, A. J., Shanks, T., Griffiths, R. E., Boyle, B. J., Almaini, O., & Roche, N. 1997, MNRAS, 291, 203
Hasinger, G., Burg, R., Giacconi, R., Hartner, G., Schmidt, M., Trumper, J., & Zamorani, G. 1993, A&A, 275, 1
Haslam, C. G. T., Salter, C. J., Stoffel, H., & Wilson, W. E. 1982, A&AS, 47, 1
Hinshaw, G., Banday, A. J., Bennett, C. L., Gorski, K. M., Kogut, A., Lineweaver, C. H., Smoot, G. F., & Wright, E. L. 1996, ApJ, 464, L25
Hogan, C. 1992, ApJ, 398, L77
Iwan, D., Marshall, R. E., Boldt, E., Mushotzky, R. F., Shafer, R. A., & Stottlemeyer, A. 1982, ApJ, 260, 111
Jahoda, K. 1993, Adv. Space Res., 13(12), 231
Jahoda, K., & Mushotzky, R. 1989, ApJ, 346, 638
Klypin, A. A., & Kates, R. E. 1991, MNRAS, 251, 41p
Lahav, O., Piran, T., & Treyer, M. A. 1997, MNRAS, 284, 499
Metzler, C. A., & Evrard, A. E. 1994, ApJ, 437, 564
Miyaji, T., & Boldt, E. 1990, ApJ, 353, L3
Miyaji, T., Lahav, O., Jahoda, K., & Boldt, E. 1994, ApJ, 434, 424
Molnar, S. M., & Birkinshaw, M. 1998, ApJ, 497, 1
Murray, S. S., Forman, W., Jones, C., & Giacconi, R. 1978, ApJ, 219, L89
Morrison, R., & McCammon, D. 1983, ApJ, 270, 119
Persic, M., Jahoda, K., Rephaeli, Y., Boldt, E., Marshall, F. E., Mushotzky, R. F., & Rawley, G. 1990, ApJ, 364, 1
Persic, M., Rephaeli, Y., & Boldt, E. 1988, ApJ, 327, L1
Piccinotti, G., Mushotzky, R., Boldt, E., Marshall, F., Serlemitsos, P., & Shafer, R. 1982, ApJ, 253, 485
Pravdo, S. H., Boldt, E. A., Marshall, R. E., McKee, J., Mushotzky, R. R., Smith, B. W., & Reichert, G. 1979, ApJ, 234, 1
Press, W. H., Flannery, B. P., Teukolsky, S. A., & Vetterling, W. T. 1986, Numerical Recipes (Cambridge: Cambridge Univ. Press)

Rephaeli, Y. 1993, ApJ, 418, 1
Rephaeli, Y., & Persic, M. 1992, MNRAS, 259, 613
Rybicki, G. B., & Lightman, A. P. 1979, Radiative Processes in Astrophysics (New York: Wiley)
Shafer, R. A. 1983, Ph.D. thesis, Univ. Maryland
Shafer, R. A., & Fabian, A. 1983, in IAU Symp. 104, Early Evolution of the Universe and Its Present Structure, ed. G. Abell & G. Chincarini (Dordrecht: Reidel), 333
Shaya, E. J., Peebles, P. J. E., & Tully, R. B. 1995, ApJ, 454, 15
Small, T. A., Ma, C.-P., Sargent, W. L. W., & Hamilton, D. 1998, ApJ, 492, 45
Snowden, S. L., et al. 1995, ApJ, 454, 643
Soltan, A. M., Hasinger, G., Egger, R., Snowden, S., & Trumper, J. 1996, A&A, 305, 17
Stark, A. A., Gammie, C. F., Wilson, R. W., Bally, J., Linke, R. A., Heiles, C., & Hurwitz, M. 1992, ApJS, 79, 77
Sunyaev, R. A., & Zeldovich, Y. B. 1980, ARA&A, 18, 537
Tully, R. B. 1982, ApJ, 257, 389
———. 1988, Nearby Galaxies Catalog (Cambridge: Cambridge Univ. Press)
Voges, W., et al. 1996, IAU Circ. 6420
White, R. A. & Stemwedel, S. W. 1992, in ASP Conf. Ser. 25, Astronomical Data Analysis Software and Systems I, ed. D. M. Worrall, C. Biemesderfer, & J. Barnes (San Francisco: ASP), 379
Yi, I., & Boughn, S. P. 1998, ApJ, 499, 198